Global Ionospheric Maps: estimation and assessment in post-processing and real-time

David Roma-Dollase

Supervisor: Prof. Dr. M. Hernández-Pajares
Prof. Dr. J.M. Gómez Cama

Aerospace Science and Technology Doctoral Program
Universitat Politècnica de Catalunya

Thesis submitted as a collection of published articles

January, 2019

UNIVERSITAT POLITÈCNICA DE CATALUNYA BARCELONATECH

Global ionospheric maps: estimation and assessment in post-processing and real-time

David Roma-Dollase

ADVERTIMENT La consulta d'aquesta tesi queda condicionada a l'acceptació de les següents condicions d'ús: La difusió d'aquesta tesi per mitjà del repositori institucional UPCommons (http://upcommons.upc.edu/tesis) i el repositori cooperatiu TDX (http://www.tdx.cat/) ha estat autoritzada pels titulars dels drets de propietat intel·lectual **únicament per a usos privats** emmarcats en activitats d'investigació i docència. No s'autoritza la seva reproducció amb finalitats de lucre ni la seva difusió i posada a disposició des d'un lloc aliè al servei UPCommons o TDX. No s'autoritza la presentació del seu contingut en una finestra o marc aliè a UPCommons (*framing*). Aquesta reserva de drets afecta tant al resum de presentació de la tesi com als seus continguts. En la utilització o cita de parts de la tesi és obligat indicar el nom de la persona autora.

ADVERTENCIA La consulta de esta tesis queda condicionada a la aceptación de las siguientes condiciones de uso: La difusión de esta tesis por medio del repositorio institucional UPCommons (http://upcommons.upc.edu/tesis) y el repositorio cooperativo TDR (http://www.tdx.cat/?locale-attribute=es) ha sido autorizada por los titulares de los derechos de propiedad intelectual **únicamente para usos privados enmarcados** en actividades de investigación y docencia. No se autoriza su reproducción con finalidades de lucro ni su difusión y puesta a disposición desde un sitio ajeno al servicio UPCommons No se autoriza la presentación de su contenido en una ventana o marco ajeno a UPCommons (*framing*). Esta reserva de derechos afecta tanto al resumen de presentación de la tesis como a sus contenidos. En la utilización o cita de partes de la tesis es obligado indicar el nombre de la persona autora.

WARNING On having consulted this thesis you're accepting the following use conditions: Spreading this thesis by the institutional repository UPCommons (http://upcommons.upc.edu/tesis) and the cooperative repository TDX (http://www.tdx.cat/?locale-attribute=en) has been authorized by the titular of the intellectual property rights **only for private uses** placed in investigation and teaching activities. Reproduction with lucrative aims is not authorized neither its spreading nor availability from a site foreign to the UPCommons service. Introducing its content in a window or frame foreign to the UPCommons service is not authorized (framing). These rights affect to the presentation summary of the thesis as well as to its contents. In the using or citation of parts of the thesis it's obliged to indicate the name of the author.

Acknowledgements

I would like to thank both of my advisors. Dr. Manuel Hernández-Pajares for his help, both at an academic level as on a personal level. This thesis would have never existed without his guidance and implication. Dr. José Maria Goméz Cama to help me to make compatible my work in the SO/PHI project with the realization of this thesis. I have learned a lot from both of them.

I would like to thank also the entire SO/PHI team at the University of Barcelona. When I started with them I had still a lot to learn and all of them have taught me, one way or another, some important lessons. Special thanks to Dr. Atilà Herms Berenguer, who gave me some very good opportunities and guided me to the correct academic direction.

I would like to thank the entire UPC-IonSAT team (current members and people that already left the team), with a special mention to Alberto, which always has assumed more work than required. It was a pleasure to work with all of you. I hope we will meet in the future in some other projects.

I am very happy to have worked with all of you, because all of you are not only good professionals, but most important, are good and kind people.

Last but not least, I also want to thank friends, family and my girlfriend for always giving me the support needed and helping me to disconnect from work.

Abstract

UNESCO codes: 120321, 220209, 250118

The research of this paper-based dissertation is focused on Global Ionospheric Maps (GIM) generation and assessment. In summary, the novelty and thematic unity in this works relies on four different but complementary topics:

- Defining a systematic procedure to validate and quantify the quality of GIMs based on independent data sources or techniques.
- Applying this methodology to not only the GIMs computed at UPC, but also to most of the currently open accessible GIMs inside the scientific community.
- Including newly available Global Navigation Satellite Systems (GNSS) data to the processing of UPC's GIMs.
- Assessment and distribution also of real-time GIMs. As a result, also a first combined real-time GIM has been implemented.

More in detail, my first contribution has been to the definition of a complete GIM validation procedure. This procedure is based on two methods: direct VTEC (Vertical Total Electron Content) altimeter and GNSS difference of slant TEC (Total Electron Content), both of them giving complementary information of the GIM performance. The main advantage of using satellite altimeter data is the fact that we are using a truly independent information source with regard to the input data used for GIM generation. This allows assessing the TEC from a entirely different point-of-view, fully different and independent to any error that may affect GNSS systems and its processing. The second technique, relies on using the same type of input data but in this case from permanent GNSS stations not participating in the GIM generation. The main advantages of this second technique is twofold: first, it allows to asses the GIMs on land; and second its a low latency direct assessment of the GIM, given a more direct information about the processing and interpolation done with the GNSS input data.

Afterwards, a second contribution has been to use the previously defined methodology to validate all the GIMs generated by the International GNSS Service (IGS) Associated

Analysis Centers (IAAC), and some other candidates to join them, for a more than a full solar cycle (starting from end of 2001 to beginning of 2017). As a side result, it is also demonstrated that while the time interval of the GIM has little influence on its overall quality, the interpolation technique used by the IAACs has an important role. Finally, this work also lead to the acceptance of the previously mentioned IAAC candidates since it demonstrated the good quality of their GIMs.

Another contribution has been, as part of the European GRC project, improving the currently in production UPC's TOMION (TOMographic IONospheric) software used to generate the UQRG (UPC's rapid GIM) map. The software input source data was restricted to GPS L1 and L2. Now it allows processing all current frequencies available for GPS, Galileo and Beidou. This software has been internally tested for some specific days with the previously explained altimeter method giving results with improved quality for specific combinations of GNSS systems and frequencies. Using this work flow but focused on single frequency processing, a last article was published analysing the ionospheric footprint of the solar eclipse over North America during 2017.

Finally, another contribution has been to improve the data acquisition and distribution system for the real-time GIM generation processing chain. Furthermore, as part of UPC contribution to the Real Time Ionospheric Monitoring Working Group (RTIM-WG) of the International Association of Geodesy (IAG) and following the previously explained methodology, an assessment of the GIMs generated by the members of this sub-commission have been performed. As a result of all these efforts, UPC has been leading inside the IGS frame, and made a first implementation, of a new real-time combined map.

Resum

Codis UNESCO: 120321, 220209, 250118

La recerca realitzada en aquesta tesis en format compendi d'articles està enfocada en la generació i validació de mapes ionosfèrics globals (GIM, del anglès Global Ionospheric Maps). En resum, la novetat i unitat temàtica d'aquesta tesis està basada en quatre temes diferents però complementaris:

- Definició d'un procediment sistemàtic per validar i quantificar la qualitat dels GIMs basada en fonts de dades o tècniques independents.
- Aplicar aquesta metodologia no només als GIMs generats a UPC, sinó també a la resta de GIMs d'accés obert actualment existent dintre la comunitat científica internacional.
- Incloure en el processat per generar els GIMs de UPC dades de les noves constel·lacions GNSS (del anglès Global Navigation Satellite Systems) disponibles.
- Validació i distribució també dels GIMs en temps real. Com a conseqüència, també s'ha aconseguit generar un primer GIM combinat en temps real.

Més en detall, la meva primera contribució va ser definir un procediment complet de validació de GIM. Aquest procediment està basat en dos mètodes: obtenció directa del contingut vertical total d'electrons (VTEC, del anglès, Vertical Total Electron Content) a partir de dades d'altimetria i per diferencies del contingut total d'electrons (TEC, del anglès Total Electron Content) inclinat de dades GNSS. Els dos donen informació complementaria de la qualitat dels GIM. L'avantatge principal d'utilitzar dades de satèl·lits altimètrics és que és una font de dades completament diferent de les que s'utilitzen per la generació dels GIMs. Aquest fet ens permet verificar el TEC des d'una perspectiva diferent, plenament independent de qualsevol font d'error que pugui afectar al propi sistema GNSS o el seu processat. El segon mètode, es basa en la mateix tipus de dades que s'utilitzen pel càlcul dels GIM però en aquest cas amb dades d'estacions permanent GNSS no involucrades en la generació dels GIMs a avaluar. L'avantatge principal d'aquest segon mètodes és doble: primer, permet avaluar el GIM sobre els continents; i segon, permet fer la anàlisis directa de baixa latència

del GIM, a més a més donant informació directa sobre el processat i la interpolació aplicada sobre les dades GNSS.

Seguidament, la meva segona contribució va ser utilitzar la metodologia prèviament definida per validar tots els GIM generats per part dels centres d'anàlisis associats al Servei Internacional de GNSS (IGS, del anglès International GNSS Service) i altres centres candidats a unir-se a IGS, per més d'un cicle solar (des de finals del 2001 fins al inici del 2017). Com a resultat secundari, també va permetre demostrar que per una banda l'interval temporal dels GIM té poca influencia sobre la seva qualitat global, però per altra banda la tècnica d'interpolació emprada per part dels centres te un impacte molt important. Finalment, aquest article va portar a l'admissió d'aquests candidats prèviament mencionats a centres d'anàlisis associats a IGS donat que es va demostrar la bona qualitat dels seus GIMs.

Una altra contribució important va ser, com a part del projecte europeu GRC, millorar el software TOMION (TOMographic IONospheric) de UPC, actualment en producció generant el GIM UQRG (GIM ràpid de UPC). Aquest software només permetia utilitzar dades de GPS L1 i L2. Les millores realitzades durant aquesta tesis permeten processar totes les freqüències actualment existent de GPS, Galileo i Beidou. El software ha estat internament validat per certs dies específics amb el mètode explicat prèviament d'altimetria millorant els resultats en comparació a la versió anterior per certes combinacions de constel·lacions GNSS i freqüències. Utilitzant aquesta nova metodologia de processat aplicada a una sola freqüència, un últim article va ser publicat analitzant l'empremta ionosfèrica de l'eclipsi solar sobre Amèrica del nord durant el 2017.

Finalment, una altre contribució va ser millorar el mètode d'adquisició i distribució del sistema de processat del GIM en temps real. És més, com a part de la contribució de la UPC, és va realitzar una validació dels GIMs generats pels participants del grup de treball de monitorització en temps real de la ionosfera (RTIM-WG, del anglès Real Time Ionospheric Monitoring Working Group) de l'associació internacional de geodèsia (IAG, del anglès International Association of Geodesy) seguint la metodologia anteriorment citada. Com a resultat d'aquestes tasques la UPC ha liderat i implementat un nou mapa combinat en temps real. en el marc de IGS.

Contents

List of Figures

List of Tables

Nomenclature

Acronyms / Abbreviations

BDS BeiDou Navigation Satellite System

CDMA Code Division Multiple Access

FDMA Frequency Division Multiple Access

GEO Geosynchronous Earth Orbit

GIM Global Ionospheric Map

GLONASS Globalnaja Nawigazionnaja Sputnikowaja Sistema

GNSS Global Navigation Satellite System

GPS Global Positioning System

IAAC IGS Associated Analysis Centres

IAAC International Associated Analysis Centers

IGS International GNSS Service

IGSO Inclined Geosynchronous Orbit

IONEX IONosphere map EXchange format

LEO Low Earth Orbit

MEO Medium Earth Orbit

NTRIP Networked Transport of RTCM via Internet Protocol

RMS Root Mean Square

RTCM Radio Technical Commission for Maritime Services

STEC Slant Total Electron Content

TAI Temps Atomique International

TEC Total Electron Content

TECU Total Electron Content Unit

UPC Universtat Politecutenica de Barcelona

VTEC Vertical Total Electron Content

Chapter 1

Introduction

1.1 GNSS Scope

Global Navigation Satellite Systems (GNSS) have an ever growing impact on large and heterogeneous sectors of human society. Its initial application as positioning has been largely overcome by other new and challenging scientific and commercial applications. In the scientific area, it is used in different applications like atmospheric sounding (Hernández-Pajares et al., 1999), space weather monitoring (Orus et al., 2007) and earthquake detection (Sagiya, 2004). As commercial application it can both be used as a precise clock, like in power grid management, and as a precise positioning system, which was its initial application. But even so, the ever better quality of the GNSS signals and understanding of the disturbances affecting them, is still opening new commercial application such as precise farming (Hernandez et al., 2017b). In summary, being able to correctly determine and understand the different delays affecting the GNSS signals is of great importance to different areas of interest.

In brief, in this section, I will make a short introduction about the signals, delays and basic terms related to GNSS.

1.2 GNSS history

The first navigation systems that can be called truly global date back to the late 1950s and early 1960s, still during the Cold War. Both the USA and Soviet Union developed similar systems, although only for military use. It was first in the 1967 that the USA made publicly available to civilians the TRANSIT system, precursor of GPS. It is interesting to notice that already on this first system the ionosphere was detected as an important error source for positioning. Hence, this first system already was transmitting at two different frequencies

to allow cancelling out its contribution. This feature has been later inherited to all modern GNSS constellations.

GPS initial operating capability was in December 1993 and fully operational at June 1995, starting the era of modern GNSS. It was originally developed for military use, but soon it was made also accessible for civilian use, although with some reduced accuracy. The second GNSS constellation to appear was GLONASS, developed by Rusia. Even when both were working in similar frequency ranges, the modulation schema used were not compatible.

In the current decade, other two GNSS constellations appeared: BeiDou (2012), from China, and Galileo, from the European Union. Galileo is still not considered fully operational although it has enough satellites already to allow navigation. It is expected to reach full operational capabilities along 2019 (Teunissen and Montenbruck, 2017).

1.3 GNSS constellations

Nowadays we can find the following four GNSS systems, sorted by initial service date (Teunissen and Montenbruck, 2017):

Global Positioning System (GPS) Property of the USA.

Globalnaja Nawigazionnaja Sputnikowaja Sistema (GLONASS) Property of Russia.

BeiDou Navigation Satellite System (BDS) Property of China.

Galileo Property of the European Union.

There are other regional satellite-based navigation systems, like QZSS (from Japan) and IRNSS (India).

GNSS systems have some common features but still are different in the details. For instance, all GNSS systems follow in some way the International Atomic Time (TAI) as a reference. But while GPS and Galileo has an offset, related to the leap seconds of its datum origin, of 19 seconds, BeiDou has an offset of 33 seconds. In this section we make a short review of their most important parameters.

1.3.1 Frequency band

In Figure 1.1, we can see the frequency allocation of the different signals transmitted by the different GNSS systems. All of them transmit at the L-band, from 1 GHz to 2 GHz, and using a right-handed circularly polarized waves. The L-band has the advantage of having a

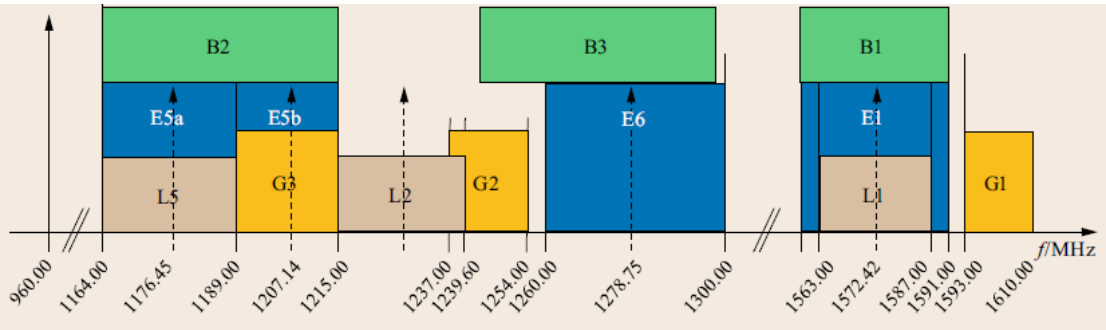

Figure 1.1 GNSS frequency bands: GPS bands in grey, GLONASS bands in orange, Galileo in blue and BeiDou in green (from Teunissen and Montenbruck (2017)).

moderate atmospheric attenuation while keeping the antenna size at an acceptable size. Also, circular polarization is preferred over linear polarization to limit the losses caused by antenna orientation mismatch.

Since the different satellites of the different constellations use the same medium for the propagation, multiple access techniques needs to be used by them. GPS started using Code Division Multiple Access (CDMA) techniques, while GLONASS used Frequency Division Multiple Access (FDMA). Even so, the new GLONASS satellites are also changing to CDMA, as do all the new GNSS systems (BeiDou and Galileo).

GNSS orbits

GPS, GLONASS and Galileo are based on a constellation of satellites at Medium Earth Orbit (MEO), around 20000 km of height (Figure 1.2). Using this height allows having an orbital period of between 11 hours 16 minutes for GLONASS up to 14 hours and 5 minutes for Galileo. The only deviation is BeiDou, which has a combination of MEO, Geosynchronous Earth Orbit (GEO) and Inclined Geosynchronous Orbit (IGSO) satellites to improve coverage for the Asian continent area. It is also worth to mention that the inclination of the other constellations is also slightly different to improve the coverage of the different countries owning the respective GNSS system.

Another parameter of interest for certain applications, as we will see later in this dissertation, is the repeatability period of the constellation geometry. This period is the time it takes for a certain receiver to see the same satellite at the exactly same relative position.

GNSS system	GPS	Glonass	Galileo	BeiDou (MEO)
Sidereal days	1	8	10	7

Table 1.1 Repeatability period of the different constellation geometry

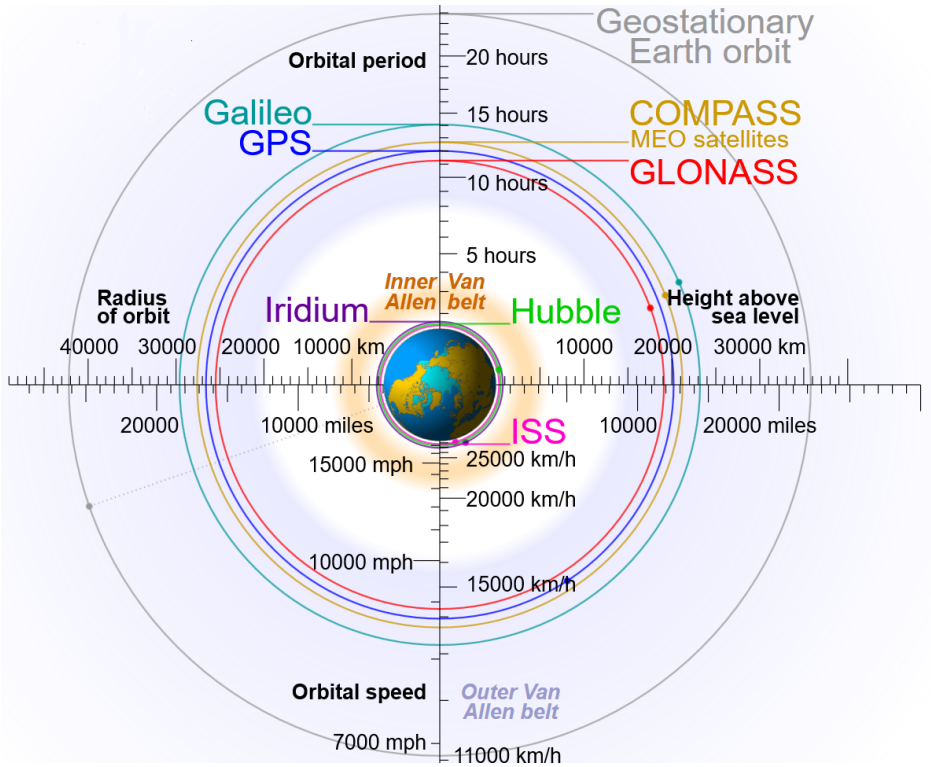

Figure 1.2 Comparison of orbital height and time between different GNSS constellations (from Wikimedia Commons (2018)).

Since this time is related with the Earth rotation, it is commonly given in sidereal days, which is the time required for the Earth to make a full rotation with regards to fixed stars. A sidereal day is approximately 23 hours, 56 minutes and 4 seconds. In Table 1.1 (Teunissen and Montenbruck, 2017) we list the the repeatability period of the different constellation geometry.

1.4 Measurements and error sources

The basic measurement made in GNSS is the apparent propagation time τ required by a GNSS signal to propagate from a given satellite to a receiver. Ideally, if we multiply this time by the propagation speed of the signal, the speed of light, we would expect to obtain the true distance between them. But, there are a lot of corrections we need to take into account in this measurement to find the true geometric distance. Therefore, the basic measurement made by the receivers is known as pseudodistances.

There are two basic measurement done by the receivers:

- Pseudorange (P): is the measure of the difference between the receiver clock reading at signal reception and satellite clock time at signal transmission multiplied by the speed of light in the vacuum.

- Carrier-phase (L): is an accumulated measure of the phase of the incoming carrier signal expressed in units of cycles of this carrier signal. The carrier phase advantage is that it reflect changes with a much higher precision than the pseudorange. But, in exchange, it includes an unknown number of integer carrier cycles due to the Doppler effect and the receiver and transmitter phase instrumental delays. And, if at some point the signal tracking is lost (cycle slip) this value is reset.

These two previous measurements can be described by the following equations, taking into account its error sources:

$$P_{k,i}^{j} = \rho_i^j + c(dt_i - dt^j) + rel_i^j + T_i^j + I_{k,i}^j + K_{k,i}^j + M_{k,i}^j + \varepsilon_{k,i}^j \tag{1.1}$$

$$L_{k,i}^{j} = \rho_i^j + c(dt_i - dt^j) + rel_i^j + T_i^j - I_{k,i}^j + B_i^j + \omega_k + M_{k,i}^j + \varepsilon_{k,i}^j \tag{1.2}$$

where:

- j refers to the satellite, i to the receiver and k to the frequency. This notation will be used along the entire dissertation.

- ρ_i^j is the true distance between satellite and receiver.

- $c(dt_i - dt^j)$ is the error due to clock differences between satellite and receiver.

- rel_i^j the relativistic effect due to space-time curvature.

- T_i^j is the tropospheric delay (neutral atmosphere).

- $I_{k,i}^j$ is the ionospheric delay.

- $K_{k,i}^j$ is the instrumental delay, which is the addition of two terms coming from the receiver and the satellite transmitter.

- $M_{k,i}^j$ is the multipath (e.g. signal reflections) related error.

- B_i^j is the phase ambiguity, including the integer number of unknown carrier cycles related to the first tracking instant and the instrumental phase delays.

- ω_k is the antenna wind-up effect.

- $\varepsilon_{k,i}^{j}$ are other unmodeled delays.

In Table 1.2 (Hernandez et al., 2005) we summarize typical values for GPS of the previous error sources.

Error source	Positioning error	Error source	Positioning error
Clock difference	$<$ 300 km	Relativistic effect	$<$ 13 m
Ionospheric delay	2 to 50 m	Tropospheric delay	2 to 10 m
Phase ambiguity	Centimetres to kilometres	Instrumental delay	Centimetres to meters
Multipath	Centimetres to decimetres	Wind-up	Below one wave-length

Table 1.2 Typical values of GPS error sources

1.5 Ionospheric delay

This PhD. thesis is focused on the ionosphere. The ionosphere is the atmospheric layer that goes from approximately 1000 km down to 50 km. In this region, the extreme ultraviolet and x-ray emissions from the Sun causes the ionization of neutral molecules and atoms, hence increasing the presence of free electrons and generating the ionospheric plasma (Figure 1.3). The internal dynamics of this plasma are very complex and strongly coupled with the magnetosphere and the solar activity. Therefore, the day and night cycle, the eleven years solar cycle or fluctuations in the Earth magnetic field among other, may produce changes up to 50 % in the electron density of the ionosphere (Teunissen and Montenbruck, 2017). Further information about this can be found in section 2.2.1.

In the previous section, we were considering that the signal path from satellite to receiver was travelling in vacuum, but for receivers on ground or low-orbit this is obviously not true. Furthermore, the atmosphere is not homogeneous and hence the signal suffers from refraction while travelling through it. To quantify this change, first we need to take into account the refractive index n, defined as:

$$n = \frac{c}{v} = \sqrt{\frac{\varepsilon\mu}{\varepsilon_0\mu_0}} \tag{1.3}$$

where c is the speed of light in vacuum, v is the speed of the signal in the given medium, ε and μ are respectively the electric permittivity and magnetic permeability in the medium and ε_0 and μ_0 are respectively the electric permittivity and magnetic permeability in vacuum. Hence, the refractive index can be directly related to the electric properties of the the medium.

Therefore, we can distinguish two regions with regards to the atmospheric delay: the ionosphere and the troposphere. There is one fundamental reason to do this distinction.

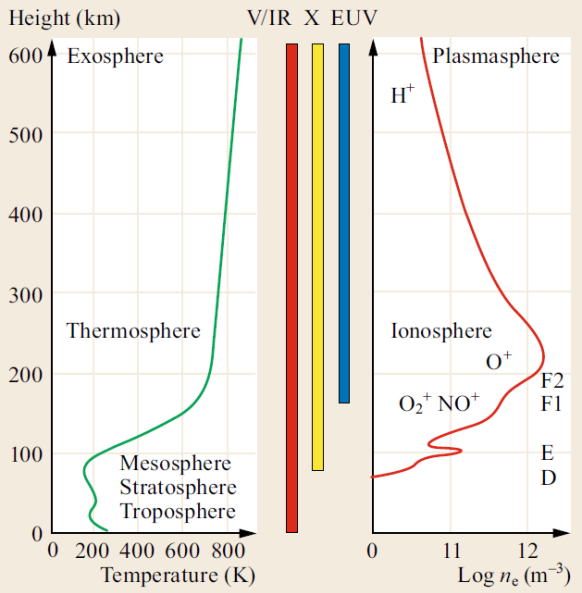

Figure 1.3 Vertical structure of the electron density of the ionosphere (right) in comparison with the neutral atmosphere temperature (left) and solar radiation penetration depths (middle), from Teunissen and Montenbruck (2017).

The troposphere, also called neutral atmosphere in this context, can be considered a non-dispersive medium. This means that its refractive index is independent of the frequency of the signal. For the ionosphere this is not true.

For GNSS, if we want to translate the refractive index to the time τ it takes for the signal to travel from satellite to receiver we can use the following equation:

$$\tau = \frac{1}{c}\int_s^r n(l)dl \tag{1.4}$$

and the delay with respect to the vacuum is then:

$$\Delta\tau = \frac{1}{c}\int_s^r (n(l)-1)dl \tag{1.5}$$

Since the code and carrier have different frequencies, the refractive index for them at the ionosphere is also different. Furthermore, it can be related to the group and phase velocity of the electromagnetic wave.

$$\begin{aligned} n_p &= \frac{c}{v_p} \\ n_g &= \frac{c}{v_g} \end{aligned} \tag{1.6}$$

where n_p is the carrier refractive index (related to the carrier-phase pseudorange) and n_g is the group refractive index (related to the code pseudorange). Both indices are related via:

$$n_g = n_p + f\frac{\mathrm{d}n_p}{\mathrm{d}f} \tag{1.7}$$

As a first order approximation in SI units (Markowitz, 1973), we can relate the carrier-phase n_p refractive index to the free electron content using:

$$n_p = 1 - \frac{40.3n_e}{f^2} \tag{1.8}$$

where n_e is the total electron content (TEC) along the path of the wave and f is the wave frequency. It is important to notice that the higher order ionospheric terms only contribute up to a 0.1 % of the total (Hernández-Pajares et al. (2014)). If we replace in (1.7) the previous expression, we find that the group refractive index is:

$$n_g = 1 + \frac{40.3n_e}{f^2} \tag{1.9}$$

Hence, we can see that the refraction index for group and carrier are equal of magnitude but with different sign. This is the reason why in (1.1) and (1.2) the value related to the ionosphere is the same but with different sign.

As noted before in (1.4), the ionospheric delay is proportional to the Total Electron Content along the path of the signal between receiver and satellite, also known as Slant Total Electron Content (STEC), hereinafter written as S in the following equations.

$$\mathrm{S} = \int_s^r n_e dl \tag{1.10}$$

The STEC is commonly expressed in TEC units (TECU) which are equivalent to $10^{16} e^-/m^2$. In this sense, 1 TECU corresponds to approximately a 16.2 cm delay for GPS L1. Using the STEC, S, we can rewrite (1.5) in terms of it as follows:

$$\Delta\tau = \frac{40.3\mathrm{S}_i^j}{cf^2} \tag{1.11}$$

And we can get the relation between the ionospheric delay at two different frequencies as:

$$I_{m,i}^j = \frac{40.3\mathrm{STEC}}{f_m^2} = \frac{f_n^2}{f_m^2} I_{n,i}^j \tag{1.12}$$

Since the STEC depends on satellite and receiver position, the vertical total electron content (VTEC, written as V in the following equations) is the value commonly distributed instead to correct the ionospheric delay in precise positioning. The VTEC, analogous to the STEC, can be defined as the integral of the electron density in a vertical columnar cylinder of unit area:

$$\mathrm{V} = \int n_e dh \tag{1.13}$$

As seen in Figure 1.3, this implies reducing the vertical 3D in a much simpler equivalent 2D distribution. In this sense, a typical shell at an effective height of 450 km is adopted for the VTEC maps. These maps, when they cover a global scale are known as Global Ionospheric Maps (GIMs). The International GNSS Service (IGS, see Dow et al. (2009)), through its International Associated Analysis Centers (IAAC), is providing this kind of maps as open products since 1998 (Hernández-Pajares et al., 2009b).

Finally, to obtain the ionospheric delay in length units from the externally obtained VTEC, a simple method is to apply an obliquity factor to account for the increase of the electronic content among the path for lower elevations, i.e. for the corresponding STEC:

$$I = \frac{1}{\cos z'} \frac{40.3\mathrm{V}}{f^2} \tag{1.14}$$

where z' is the zenith angle of the satellite with regards to the so-called ionospheric pierce point, which is the point where the line-of-sight vector between satellite and receiver crosses the ionospheric thin shell of the VTEC. For more details, see section 19.3 of Teunissen and Montenbruck (2017).

1.6 GNSS combinations

1.6.1 Ionosphere free combination

As already explained before, historically, the ionospheric delay was difficult to assess and hence the GNSS satellite were, and still are today, emitting signals at more than one frequency. Hence, using (1.1), (1.2) and (1.12), the so-called ionospheric free-combinations (*PC* for the pseudorange and *LC* for the carrier-phase) can be made to remove the effect of the

ionosphere:

$$\begin{aligned} PC_i^j &\equiv \frac{f_1^2 P_{(1,i)}^j - f_2^2 P_{(2,i)}^j}{f_1^2 - f_2^2} \\ &= \rho + c(dt_i - dt^j) + rel_i^j + T_i^j \\ &+ \frac{1}{f_1^2 - f_2^2}\{f_1^2(K_{1,i}^j + M_{1,i}^j + \varepsilon_{1,i}^j) - f_2^2((K_{2,i}^j + M_{2,i}^j + \varepsilon_{2,i}^j)\} \end{aligned} \tag{1.15}$$

where the corresponding instrumental delays are defined as zero for actual P_1 and P_2 GPS.

$$\begin{aligned} LC_i^j &\equiv \frac{f_1^2 L_{(1,i)}^j - f_2^2 L_{(2,i)}^j}{f_1^2 - f_2^2} \\ &= \rho_i^j + c(dt_i - dt^j) + rel_i^j + T_i^j + B_i^j \\ &+ \frac{1}{f_1^2 - f_2^2}\{f_1^2(\omega_1 + M_{1,i}^j + \varepsilon_{1,i}^j) - f_2^2(\omega_2 + M_{2,i}^j + \varepsilon_{2,i}^j)\} \end{aligned} \tag{1.16}$$

On the other hand, if we only have single-frequency observations, the GRAPHIC combination can be used instead. The GRAPHIC combination (O_{GPH}) takes advantage of the opposite of the sign between carrier-phase and pseudorange present at the ionospheric dependency:

$$\begin{aligned} O_{GPH,i}^j(t) &\equiv \frac{1}{2}(P_{k,i}^j(t) + L_{k,i}^j(t)) \\ &= \rho_i^j + c(dt_i - dt^j) + rel_i^j + T_i^j + \\ &\frac{1}{2}(K_{k,i}^j + B_i^j + \omega_k + M_{k,i}^j + M_{P,k,i}^j + M_{L,k,i}^j + \varepsilon_{P,k,i}^j + \varepsilon_{L,k,i}^j) \end{aligned} \tag{1.17}$$

where P_k and L_k are the pseudorange and carrier phase at a given frequency f_k respectively and both in length units, j refers to the satellite and i is the receiver. The other terms are the same than defined at equations 1.1 and 1.2. As we can see in this way we get rid of the ionospheric effect but in exchange we add all the noise sources of carrier phase and pseudorange, although divided by a factor two. Specially relevant is that we now have also the phase ambiguity and the pseudorange multipath present, which needs to be estimated in positioning applications. But the ambiguity, along an arc of observation, can be considered constant.

1.6.2 Ionospheric combination

For applications where the focus is on the ionosphere instead, for dual frequency receivers we can perform the ionospheric combination (also called geometric free combination) for pseudorange (*PI*) and carrier-phase (*LI*) using equations (1.1), (1.2) and (1.11):

$$\begin{aligned} PI_i^j &\equiv P_2 - P_1 \\ &= 40.3\left(\frac{1}{f_2^2} - \frac{1}{f_1^2}\right)\mathrm{STEC}_i^j \\ &+ (K_{2,i}^j - K_{1,i}^j) + (M_{2,i}^j - M_{1,i}^j) + (\varepsilon_{2,i}^j - \varepsilon_{1,i}^j) \end{aligned} \tag{1.18}$$

$$\begin{aligned} LI_i^j &\equiv L_1 - L_2 \\ &= 40.3\left(\frac{1}{f_2^2} - \frac{1}{f_1^2}\right)\mathrm{STEC}_i^j \\ &+ (B_{2,i}^j - B_{1,i}^j) + (m_{2,i}^j - m_{1,i}^j) + (\omega_{2,i}^j - \omega_{1,i}^j) + (\varepsilon_{2,i}^j - \varepsilon_{1,i}^j) \end{aligned} \tag{1.19}$$

The order of the frequencies sub-index between (1.18) and (1.19) is inverted to take into account the different sign of the ionospheric delay between carrier-phase and pseudorange.

If we only have single-frequency observations, we can perform an equivalent combination to the previously explained GRAPHIC, the so-called iono-GRAPHIC (IG) combination:

$$\begin{aligned} I_{GPH,i}^j(t) &\equiv \frac{1}{2}(P_{k,i}^j(t) - L_{k,i}^j(t)) \\ &= I_{k,i}^j(t) \\ &+ \frac{1}{2}(K_{1,i}^j - B_{1,i}^j - \omega_{k,i}^j + M_{k,i}^j - m_{k,i}^j + \varepsilon_{k,i}^j) \end{aligned} \tag{1.20}$$

Again, as happens with the GRAPHIC combination, I_{GPH} also suffers from an increase in noise sources which includes the carrier-phase ambiguity.

1.7 Global Ionospheric Maps

Global Ionospheric Maps have been computed and openly provided in the frame of IGS since June 1998 (Hernández-Pajares et al., 2009b). They contain the worldwide distribution of the VTEC with a typical spatial resolution of $5^\circ \times 2.5^\circ$ and 2 hours temporal resolution. The GIMs are typically estimated from a hundred of worldwide permanent GNSS receivers,

gathering thousands of dual-frequency observations. Depending on the latency of these GIMs they can be classified as real-time (RT), with a latency less than 15 min; rapid, with a latency of up to one day; and final, with a typical latency between one and two weeks. The traditional way to distribute them has been through the IONEX format (Schaer et al., 1998). More recently, for the real-time GIMs, the Networked Transport of RTCM via Internet Protocol (NTRIP) has a specific message for the distribution of ionospheric information. Also, instead of using the longitude and latitude grid as does the IONEX files and sending directly the VTEC information, this message contains the spherical harmonics coefficients of the GIM instead. The advantage of using the spherical harmonics is that the bandwidth needed to transmit the information is minimized, but this comes in exchange with a certain loss of information.

Different estimation techniques have been developed by different ionospheric analysis centres, in particular for the slant-to-vertical mapping, with the general assumption of a common worldwide effective height or, alternatively, a tomographic description (Hernández-Pajares et al., 1999)) and an associated new mapping function (Lyu et al., 2018). Regarding the very important aspect of interpolation, different techniques are used, like the spherical harmonic expansions (Schaer, 1999), and combined with generalized trigonometric series functions (Li et al., 2015), Spline (Mannucci et al., 1998) and Kriging (Orús et al., 2005). A more detailed comparison of the different methods can be found at Hernández-Pajares et al. (2017)

Chapter 2

Summary of the work performed

The present chapter summarizes the main contributions obtained in the context of my Ph.D. study. Most of the results presented in the following sections have been validated by the international scientific community through the assessment of papers published in peer-reviewed journals and international conference proceedings. A selection of quality indexes for each journal can be found in Chapter 3 and the original manuscripts are appended at Chapter 5.

2.1 GIM validation methodology

The first important step performed has been to define a GIM assessment methodology. The importance of this step is double: first, to assess the relevance of the changes made to the internal GIM computation methodology and second, to compare in a fair way the performance of the different IAACs GIM.

From an internal point-of-view, the interest of this work was for the following reasons:

- Optimization of different computation parameters, like for example the input data sampling rate or the required station coverage density. Both parameters have an important impact to the computational effort required, hence impacting in the resource usage and latency of the generated maps. It is therefore important to use the minimum required number while keeping the GIM degradation at an acceptable level.

- Incorporation of new GNSS signals. The first version of the UPCs GIM computation software (TOMION) did only use GPS data. Due to the current increase of available GNSS systems, which means at least an increase in the reliability of the software depending on them, it was of large interest to include other GNSS systems data.

Having a well defined methodology is, in this sense, critical to validate that this step was really providing better maps.

From the point-of-view of the IGS ionospheric community, it was interesting to have a methodology to be able to compare the large diversity of existing GIM computation methodologies. Also, new institutes have started producing new GIMs and hence were not included in the combined IGS GIM. And since the combined IGS GIM is mostly based on the fair assessment of the consistency and accuracy of the individual GIMs, it was of interest to make an assessment including both.

The key points on which this methodology is based are:

- Independent: The GIM assessment methodology includes other data types directly related to the TEC but not included in GIM computation. Furthermore, when the data type is the same, it does not use the same data source.
- Well established: The methodology uses well-defined and established techniques from previous works, avoiding the risk of including undefined bias or not having quality data providers.
- Global coverage: The methodology is able to assess the quality of the GIM at a global scale and not only at some regions. This allow to compare the GIMs at both high developed and inhabited regions, with usually lots of input data, and places like the Earth poles or the oceans, where the number of input data sources is scarce, if any.

The methodology presented in Hernández-Pajares et al. (2017) hence is based on two techniques:

- VTEC altimeter: Dual-frequency altimeters, such a TOPEX and the JASON satellites, providing a direct measure of the VTEC below them. The altimeter is of special interest since it is not used in current GIM computation. Its downsides are that it does not include the topside electron content (which is usually much smaller than the GIM discrepancies and hence can be neglected) and that it only provides coverage over oceans. But the later can be also considered an advantage, since we are analysing the performance of the GIMs in a more difficult place, usually further away from permanent station. This kind of measurements are still a bit noisy, hence a sliding window smoothing of 16 seconds data is applied to bring the standard deviation error down to 1 TECU.

- dSTEC GPS: Comparison with the STEC variation along a phase-continuous transmitter–receiver arc above the horizon with regards to its STEC at maximum elevation obtained from permanent GPS stations. This method provides accuracies better than 0.1 TECU. It is a variation of the one used since 1998 for ranking, weighting and combining the GIMs of IGS centres. Hence, it is a well-established method. Furthermore, we are explicitly filtering out the stations involved in the computation of any GIM being assessed. This ensures that we are performing an independent assessment.

Finally, in this work, the methodology was applied to a set of 26 permanent GPS receivers located on islands. Afterwards, a comparison of both results was carried out, demonstrating the correlation of both methods. This correlation is a further evidence that both data are providing information about the same physical quantity, the TEC.

2.2 Assessment

The previous defined methodology of dSTEC and dual-frequency altimeter assessment was used to analyse the GIMs of the IAAC and new IAAC candidates from end of 2001 to beginning of 2016. The results were published in Roma-Dollase et al. (2018b).

A first part of this paper, provided by the co-authors of the different institutes, explains their methodology for the GIM computation. In Table 2.1, extracted from the paper, a summary of the different GIMs is shown. We can see that there are two main methodologies for the computation: spherical harmonics and tomographic interpolation. Another interesting aspect, is that the DCBs are usually estimated at the same time as the VTEC. The only IAAC

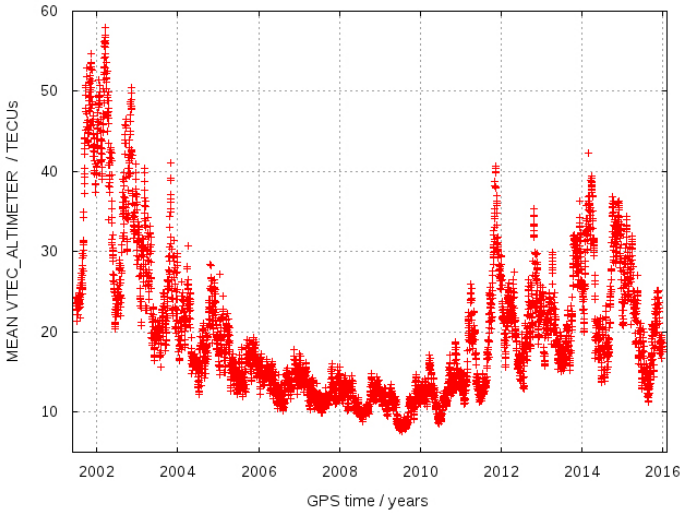

Figure 2.1 Daily altimeter mean VTEC during a whole solar cycle

Table 2.1 Summary of the different GIMs assessed.

GIM ID	Method	DCB Computation	Shell Model	Start Date	Ref.
IGSG	Weighted Mean	Combined	Combined	1998.4	Hernández-Pajares et al. (2009a)
CODG	Spherical Harmonics	Same time as VTEC	Modified 2-D	1998.4	Schaer (1999)
ESAG[1]	Spherical Harmonics	Same time as VTEC	2-D	1998.4	Feltens (2007)
JPLG	Three-shell Model	Same time as VTEC	3-D	1998.4	Mannucci et al. (1998)
UPCG	Tomographic with splines	From VTEC	3-D	1998.4	Hernández-Pajares et al. (1999)
UQRG,3[2]	Tomographic with kriging	From VTEC	3-D	2011	Orús et al. (2005)
CASG	Spherical Harmonics and Generalized Trigonometric Series	Same time as VTEC	2-D	2016	Li et al. (2015)
EMRG[3]	Spherical Harmonics	Same time as VTEC	2-D	1998.4, 2015.3	Ghoddousi-Fard (2014)
WHRG[3]	Spherical Harmonics and Inequality-constrained Least Squares	Same time as VTEC	2-D	2016	Zhang et al. (2013)
WHUG	Spherical Harmonics and Inequality-constrained Least Squares	Same time as VTEC	2-D	2016	Zhang et al. (2013)

that doesn't follow this approach, since it uses a tomographic approach based on carrier phase data only, is UPC. In this case first the GIM is calculated and afterwards the DCBs are estimated from the VTEC data.

As previously mentioned, the assessment covers an almost 14 year time span. From the altimeter daily mean VTEC, the solar cycle and seasonal oscillations are observable (Figure 2.1). This ensures that the assessment will not cover only a specific time span where

[1] A 3D multi-layer assimilation model is currently under development by ESA.

[2] The time interval of UQRG is fifteen minutes, in contrast with the other GIMs which have a time interval of two hours.

[3] UQRG, EMRG and WHRG are rapid GIMs with a latency of less than two days, in contrast with the other final GIMs which have a latency about one week.

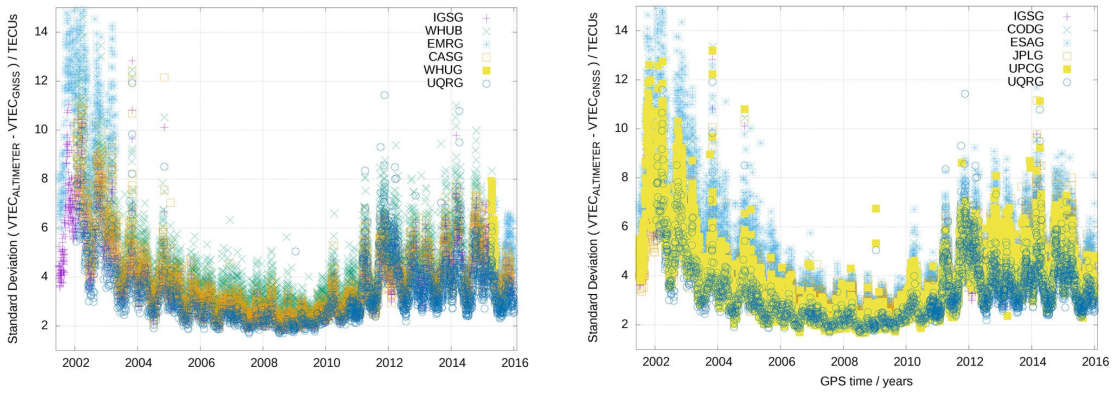

(a) Newer IAACs

(b) IAACs since 1998

Figure 2.2 Daily standard deviation of the VTEC difference regarding altimeter VTEC measurements. UQRG and IGSG has been plotted on both figures for a common reference.

the conditions may be more favourable to one of the GIMs, at the contrary, it covers very different ionospheric level periods.

2.2.1 Dual-frequency altimeter results

The results of the assessment can be seen in Figure 2.2. As a first result, it can be seen that the error of the GIMs is also dependent of the solar activity cycles. This was already expected due to the increase of the mean global TEC value. On periods of a more calm ionosphere, the error goes down to 2 TECUs, while on higher level periods it can rise up to 10 TECUs, depending on the GIM used.

Table 2.2 summarizes the VTEC-altimeter results for the full period and for a shorter time span, common for all the GIMs compared. The results shows that the new IAAC candidates perform from this analysis similarly than the classical IAACs.

2.2.2 dSTEC-GPS results

The dSTEC-GPS, as required in the previously defined methodology, was done over a common set of stations not used in the GIM computation of any of the IAACs. Since this was not feasible to be done for the entire time span, the two solstice and two equinox days of 2015 were used (days 082, 146, 280 and 330). The mean value of the dSTEC root mean square (RMS) relative error per stations was used for the analysis. Finally, these stations' mean values were interpolated to make easier to see the spatial distribution of the error (Figure 2.3).

A degradation of the GIM quality for high latitude and low latitude (in coincidence with the equatorial anomaly) can be seen. This degradation is expected to be related to the higher

Table 2.2 Summary of the GIMs assessment vs +190 millions of altimeter VTEC measurements, including an overall period of up to almost 5000 days and a common period of 21 days.

	Up to more than 1 Solar Cycle, within days 180, 2001 to 007, 2016			21 common days, within 117, 2015 to 007, 2016	
GIM Id.	# days	Std. Dev. / TECU	Rel. Error %	Std. Dev. / TECU	Rel. Error %
IGSG	4927	3.9	19.9	4.6	21.1
CODG	4934	4.3	22.0	4.8	21.8
ESAG	4926	5.3	26.6	5.6	25.5
JPLG	4912	4.1	21.2	4.8	21.9
UPCG	4925	3.9	19.7	4.2	19.1
CASG	4914	3.9	20.9	4.6	21.1
EMRG	255[*]	(4.8)	(26.2)	5.9	26.5
WHRG	4416	4.6	24.8	5.5	25.0
WHUG	42[**]	(5.9)	(26.9)	5.5	25.0
UQRG	3063	3.6	17.8	3.6	16.3

([*] For the newest period of EMRG product submission to IGS only, days 117-365, 2015; [**] Very limited sample)

ionospheric variability in these regions. Furthermore, also a higher error can be seen on most GIMs at the Southern Hemisphere. This is most probably due to the lower availability of receivers in this region.

2.2.3 Conclusions

The results of this paper showed the GIM accuracy and its evolution over a large time span. Furthermore, an important side results for the IGS community, was that it shows that the new centres providing GIMs have an accuracy similar to the classical IAACs. This has allowed including these GIMs to the combined IGS GIM, allowing an increase in reliability, accuracy and community around the IGS GIM.

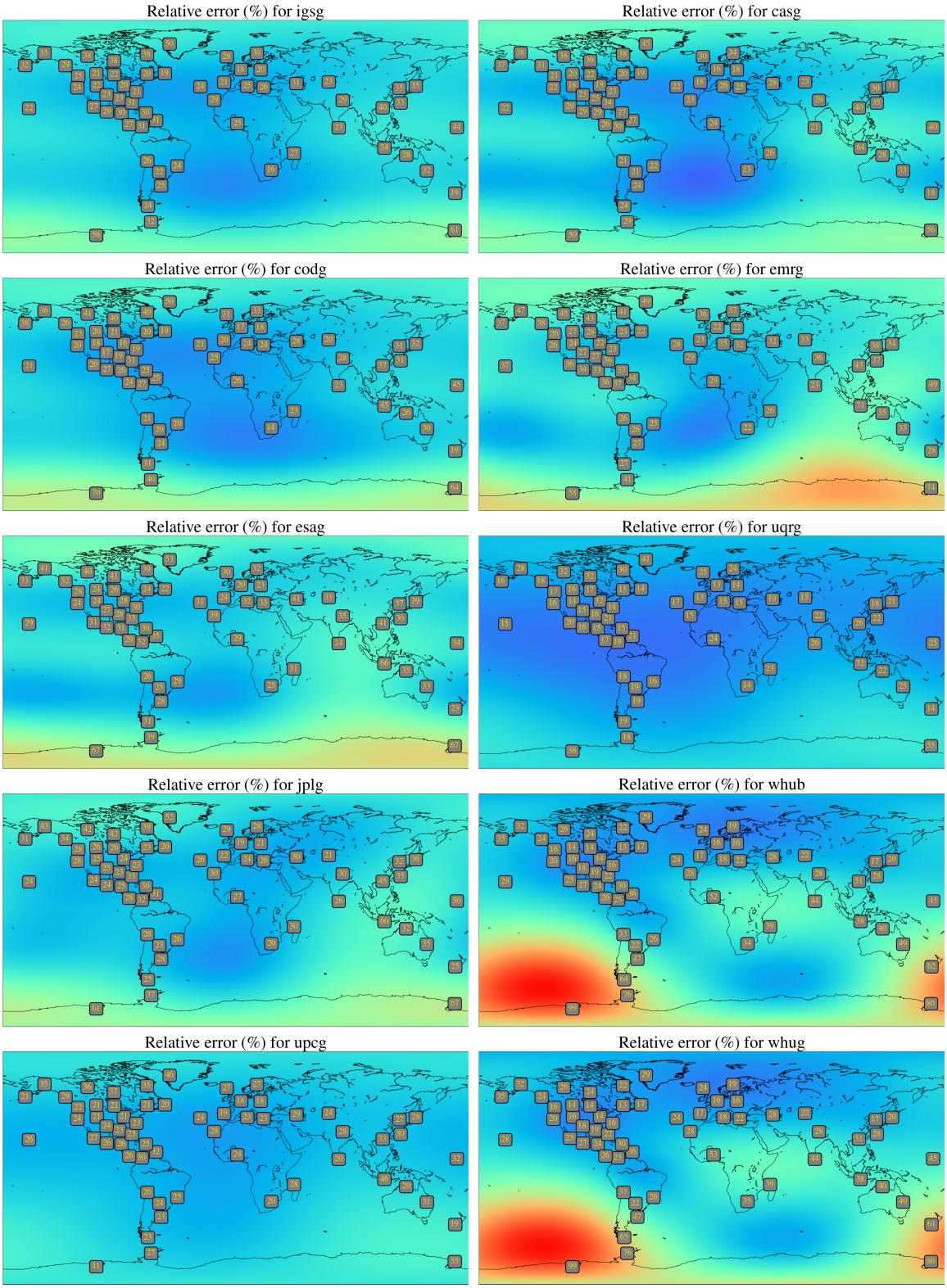

Figure 2.3 Map approximating the spatial distribution of dSTEC relative error for classical IGS GIMs (left hand column, for IGSG, CODG, ESAG, JPLG and UPCG from top to bottom) and new GIMs (right hand one, for CASG, EMRG, UQRG, WHRG andWHUG from top to bottom). Color red represents an error of 100% and dark blue of 0%

2.3 Improvements towards a multi-GNSS GIM

Another important work developed during this thesis have been updating the current TOMION (Tomographic Ionosphere model) software, responsible of the generation of UPCs GIMs. The previous version of TOMION was using only GPS data. It was considered due to the scientific interest to make TOMION capable of using other GNSS data, specially in case of Galileo data. The updated TOMION software is being useful as well in new and on-going projects such as the Galileo Reference Centre (GRC) project, lead by GMV, which will provide information of the Galileo status to the the European GNSS Agency (GSA, formerly Galileo Supervisor Authority).

To minimize the maintenance and keep the large heritage from TOMION, the approach selected was to modify the input data of the different GNSS systems in such a way that the core software of TOMION was kept intact. Furthermore, it was decided that there should be always the option to fine tune which constellations, frequencies and signals may be used.

Taking all this into account, it was decided that the best approach will be to modify the input data in such a way that for TOMION all the input data will look like GPS data and that its constellation has grown up to 100 satellites. This was done adding an offset to the satellite identifier of all constellation except to GPS. Since currently Glonass still uses FDMA in some satellite (in contrast with all the other GNSS constellations which are CDMA), it was currently discarded, since it will imply changes to the core functions of TOMION. Hence, the current offsets implemented are 32 for Galileo and 64 for Beidou.

In summary, the following changes were implemented in TOMION:

- Definition of a new variable, both for GIM and DCBs generation, to select the constellation, frequency and signal. It is important to notice that TOMION is based on the dual-frequency ionospheric combination *LI* (Eq. 1.19). Hence, this variable defines both frequencies and signals from the same constellation. It was decided that it will be a list and the syntax of its entries will be in the format *E_L1_L5A_C_Q*, where the first letter refers to the constellation, the second and third field separated by the underscore are the two frequencies to combine and the four and five field, which are optional, tells the signals from the corresponding frequency. In case this last fields are not defined, all signals from the frequency will be used. These behaviour, specially for the computation of the DCBs, is not recommended but is kept to reproduce the previous behaviour of TOMION.

- Use of the new RINEX version 3 files. TOMION was only capable of processing RINEX v2 files. But the RINEX v2 standard was only defined taking into account GPS and Glonass. Still, some files which may also include Galileo may be found, but

this may have been insufficient to generate a GIM only from Galileo data, which was considered to be necessary. In this sense, and since at some point the multiconstellation RINEX files needs to be splited in one file for every constellation data they contain, the *gfzrnx* software from GFZ Potsdam Nischan (2016) was decided to be used. This software allows doing all this steps at once: filter constellation and signals and conversion from RINEX version 3 to version 2.

- Usage of the new multi-constellation broadcast ephemerides file (BRDM). TOMION was using BRDC navigation files. But, similarly to RINEX v2, these files only include GPS ephemerides data, we needed to change the input navigation files to BRDM. As before, these files are later converted to multiple BRDC files, one for each constellation.

- The generated RINEX v2 and BRDC files for each constellation are the processed separately to compute the different combinations the same way we processed the GPS data but with the appropriate frequencies. Then, before the tomographic computation begins, all of them are merged applying the offset to each specific satellite identifier and scaled to the LI_{L1-L2} combination. This way, we have a file with all the observations in the same units as the original TOMION *LI* combination and with a number of satellites that can go up to 100.

- Due to the increase in stations and constellations it was considered important to parallelize the input processing. In this sense, the GNU Parallel software (Tange, 2018) was used. The results is that for a similar number of stations (but a larger constellation), were the original TOMION version required more than 20 hours, the current version only requires 5 hours.

An in-depth assessment of the new multi-GNSS TOMION is still required, but first results show that the resulting GIM using Galileo only data has a lower bias compared to GPS, while the standard deviation is similar. For Beidou, it is not currently feasible to generate a GIM due to the low number of receivers and satellites. Still, the combined GPS and Galileo map shows an improvement in both bias and, although in a almost negligible degree, standard deviation. Furthermore, using both constellations allows having a much larger set of stations and observations, hence not only affecting accuracy, but also improving the reliability and global coverage.

Finally, a more thorough testing was done for the DCBs computed with this methodology. The results show a good agreement with the DCBs computed by DLR (Fig. 2.4), with a mean difference below 0.1 ns for most satellites and below 1 ns for common permanent stations. The error bars provided by TOMION are very pessimistic, but this was already the case for the previous version.

2.4 Sidereal Day Filtered Ionospheric Graphic Combination

In the last paper, Hernández-Pajares et al. (2018), the previously explained multi-GNSS procedure was used to validate a new observable combination. This new combination, called sidereal days ionospheric graphic (δI_g), may be specially useful for using single-frequency receivers for ionospheric sounding. δI_G is an evolution of the previously introduced ionospheric GRAPHIC combination (1.20). But in this case we take advantage that, taking into account the repeatability period of the different GNSS constellations (Table 1.1), for a permanent station (or any static receiver) the terms related to the geometry and other that can be considered constant between measurements, cancel out when computing the difference. The only remaining terms are:

$$\delta I_{G_i}^j(t) = \frac{K}{f^2} M_i^j(t) \cdot \delta V_i^j(t) + \frac{1}{2}\left(-\lambda_1 \delta N_{1,i}^j + \delta v_{1,i}^j(t)\right) \tag{2.1}$$

where K is a constant with value 40.3 m^3/s^2 (Hernández-Pajares et al., 2011), f is the frequency of the signal, M is the mapping function, δV is the VTEC difference, λ is the wavelength of the signal, δN is the difference between the cycles from the continuous arc measurement and δv is the thermal noise difference of the measurements. The term related to the cycles can be calibrated, and in the paper two different methods are explained in depth.

This technique has been applied to detect the ionospheric footprint of the total solar eclipse over North America happened during the 21^{th} of August, 2017. One multi-GNSS and nine GPS permanent station data were also compared in order to detect the solar eclipse footprint. The equivalent results, with Galileo-only and GPS-only respectively, can be seen in Fig. 2.5. The VTEC depletion during the eclipse can be clearly seen, even for the Galielo

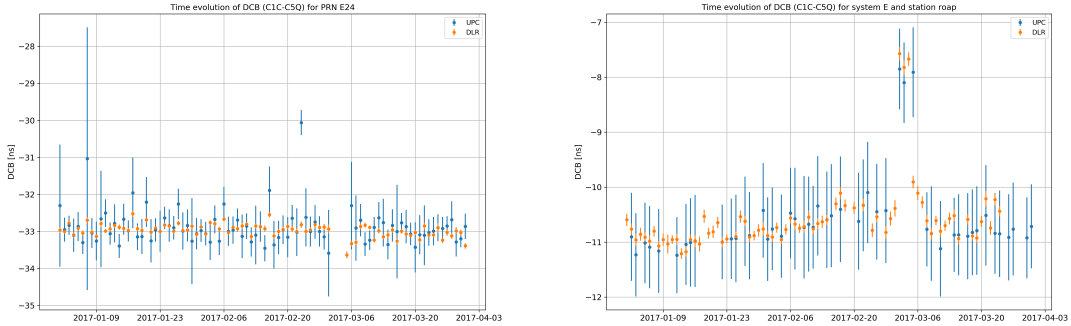

Figure 2.4 DCBs comparison between the values provided by DLR and computed with the new TOMION version

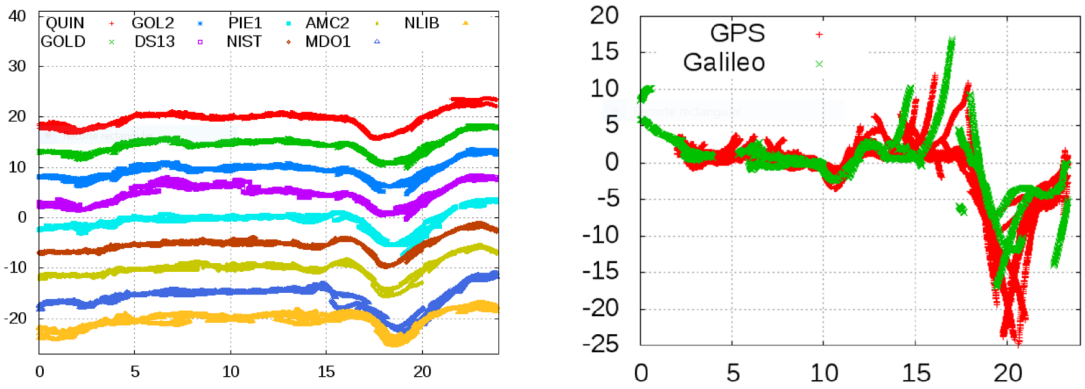

(a) VTEC difference for the GPS receivers

(b) VTEC difference for SCUB receiver

Figure 2.5 VTEC difference with regards to one sidereal day for the GPS receivers and 10 sidereal days for the SCUB receiver.

data of the GNSS receiver where instead of one sidereal day ten have been used due to the repeatability period of hte Galileo constellation.

Finally, in the paper some other interesting factors which may affect the δI_G combination have been analysed, like the possible corrections of cycle-slips and, most interesting due to its cost and availability, the usage of a mass market receiver in both high and low latitude situations. It concludes that the proposed combination is fully compatible with the usage of this kind of receivers with a similar performance as with high end geodetic dual-frequency receivers.

2.5 Real-Time GIMs

2.5.1 Data acquisition

To improve the quality of the real-time maps produced at UPC it was necessary to update the number and distribution of the permanent stations from which data was fetched. The real-time GNSS data is commonly distributed using the NTRIP protocol. This protocol defines three levels:

- Server: the server streams data to a caster. This data can be, for example, observables from a GNSS receivers or clock corrections to be send to precise-positioning users.
- Caster: gets the data streams from the different servers and allows accessing them by the users. It also implements authentication to allow only accessing the data by the users with the right credentials.

- Client: connects to a caster and gets the data from the different mount-points (e.g., the servers) of interest by the user.

In our case, since we only wanted to get the observables data from permanent stations, we only needed a NTRIP client. As it is free of charge and its widespread usage, we decided to use the BKG's NTRIP Client (BNC) software.

Afterwards, the following step was searching the Internet to increase the number of NTRIP casters we had access. Then, an XML file was written with all casters we had access and the authentication information to them. Then, a python script was created to classify all the station available through the casters and generate a final configuration file for the BNC software.

To classify the mount-points we had access through the casters, the BNC software is run in batches with a set of them. This is done to avoid stability problems with BNC due to the high amount of mount-points (currently more than 1500). Afterwards, the output produced is analysed to classify the mount-points that have least time gaps. Then, the most reliable stations are selected verifying that no other previous selected station is below a threshold distance. The distance between them is calculated following a great circle approximation. This distance is configurable but, from previous studies, it is required to be around 450 km (Valls-Moreno, 2008). Furthermore, the results of the classification is stored in a file, in such a way that in following runs these results are included scaled by a time related factor. This allows that in case that a station is in the current moment not available, for instance due to maintenance, but in the past was highly reliable, may be still included. All these options are fully configurable, or even can be fully disabled, depending of command line arguments given to the tool. In Figure 2.6, we can see an example of the resulting map of selected stations.

Finally, the full data acquisition chain was improved to make it more reliable and stable. This system has been stable for months, even correctly restarting itself at system booting after power cuts.

2.5.2 Assessment

A similar methodology defined by the GIMs generated with post-processing information was applied to assess some real-time and near real-time GIMs. The real-time GIMs compared where the ones produced by UPC, the Centre National d'Etudes Spatiales (CNES) and the Chinese Academy of Science (CAS). Only one near real-time GIM was included, the one computed by the Technische Universität München (TUM). To compare the performance of these GIMs with the post-processing ones, also the post-processing GIM computed by UPC

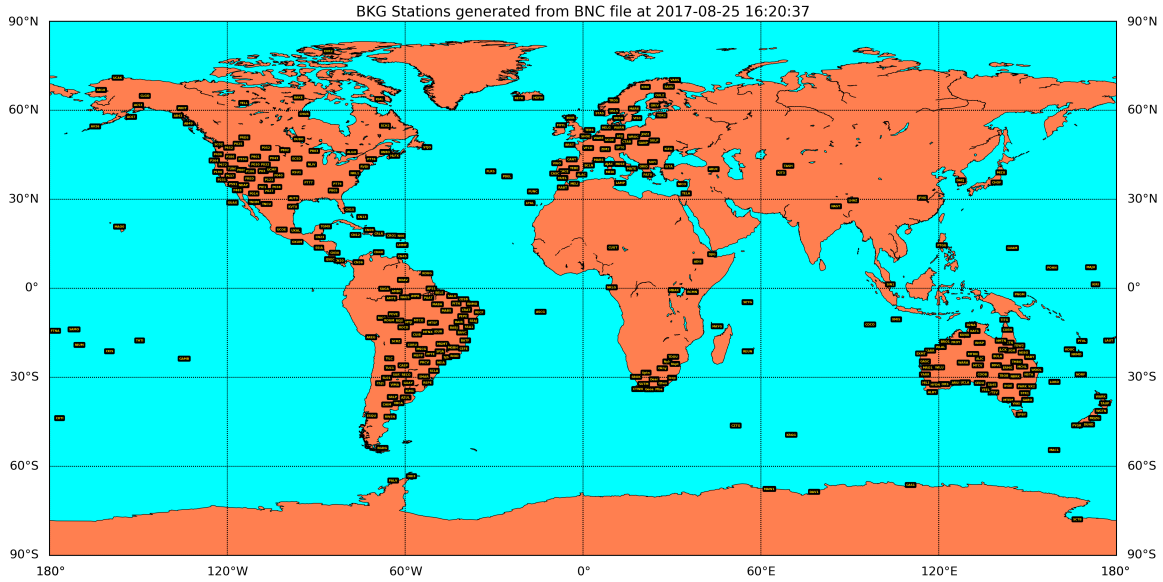

Figure 2.6 Real-time stations map

and the IGS combined GIM were included in the assessment. The full results were published in (Roma Dollase et al., 2016).

They show that in places like Europe, where a dense real-time station network is present, the performance of some of the real-time GIMs is similar to the post-processing GIMs. But at a global scale, the performance of the post-processing GIMs is almost two times better for both the altimeter and dSTEC test.

2.5.3 Distribution

The standard way of distributing the VTEC information in real-time is using RTCM message 1264. This VTEC information is provided using a spherical harmonics cosine and sine expansion (Eq. 2.2).

$$VTEC(\Phi_{pp},\lambda_{pp}) = \sum_{n=0}^{N}\sum_{m=0}^{min(n,M)} (C_{nm}\cos m\lambda_s + S_{nm}\sin m\lambda_s)\, P_{nm}\sin\Phi_{pp} \qquad (2.2)$$

where N and M are the degree and order respectively of the spherical harmonics, C_{nm} the cosine coefficients, S_{nm} the sine coefficients, λ_s mean sun fixed longitude phase shifted by 2 h of the ionospheric pierce point for the layer modulo 2π, λ_{pp} longitude of ionospheric pierce point for the layer, Φ_{pp} geocentric latitude of ionospheric pierce point for the layer and P_{nm} the fully normalized associated Legendre functions.

The main problem we found with this message is that the standard limits the maximum order and degree to 16. In Figure 2.8 we can see the effect of using different order and degrees. For instance, when using order and degree of eight, the Southern Hemisphere anomaly peak separation has completely disappeared. For order and degree 16, the map visually reproduces correctly the original IONEX file, but it can be appreciated some extra smoothing at some areas. Using the UQRG (UPC's rapid GIM) IONEX files for a set of a few days, we did the same process again and computed the RMS difference to the original map (Figure 2.7). All this results were presented at Hernandez et al. (2017b).

Taking into account these results we decided to use the maximum possible order and degree defined by the standard. Then, an NTRIP server was created again based on the BNC software. Another python script continuously computes the hash of the latest URTG (UPC's real-time GIM) IONEX file. When the hash changes, the script reads the latest map present and computes the sine and cosine spherical harmonics coefficients of the GIM. If the conversion is successful, the internal stored map is updated. This is done to avoid problems reading a truncated file. Afterwards, this internal map is send via TCP to an instance of the BNC software in RTNET format. The BNC then connects to an internal NTRIP caster running inside UPC premises and externally accessible. It is planned in a near future to send this data direct to the IGS real-time products caster.

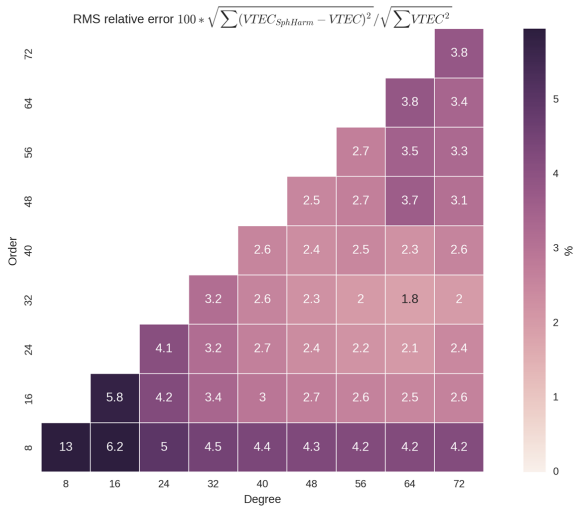

Figure 2.7 RMS of the error for a group of maps expanded for a different number of order and degrees

2.5.4 Combined real-time GIM

UPC has been leading the effort inside IGS with success to generate a combined real-time GIM. The current process consist of two main parts: a first data acquisition software and a second weighting and combining software. The data acquisition software is, due to the experiences already previously explained in this section, based on the BNC software. The BNC software currently acquires the real-time GIMs of UPC, CNES and Wuhan University. Then, another script converts the different spherical harmonics map in separated IONEX files and also generate some other files with meta-data information required by the following processing step. The weight of the GIMs is done using the normalized inverse of the squared RMS error obtained by the dSTEC test of 20 receivers. The combination is done then directly applying this weight on the different GIMs and adding them. The resulting combined map was assessed against the VTEC-altimeter test and frequently shows a better performance than the different original GIMs. This results were shown at Roma-Dollase et al. (2018a).

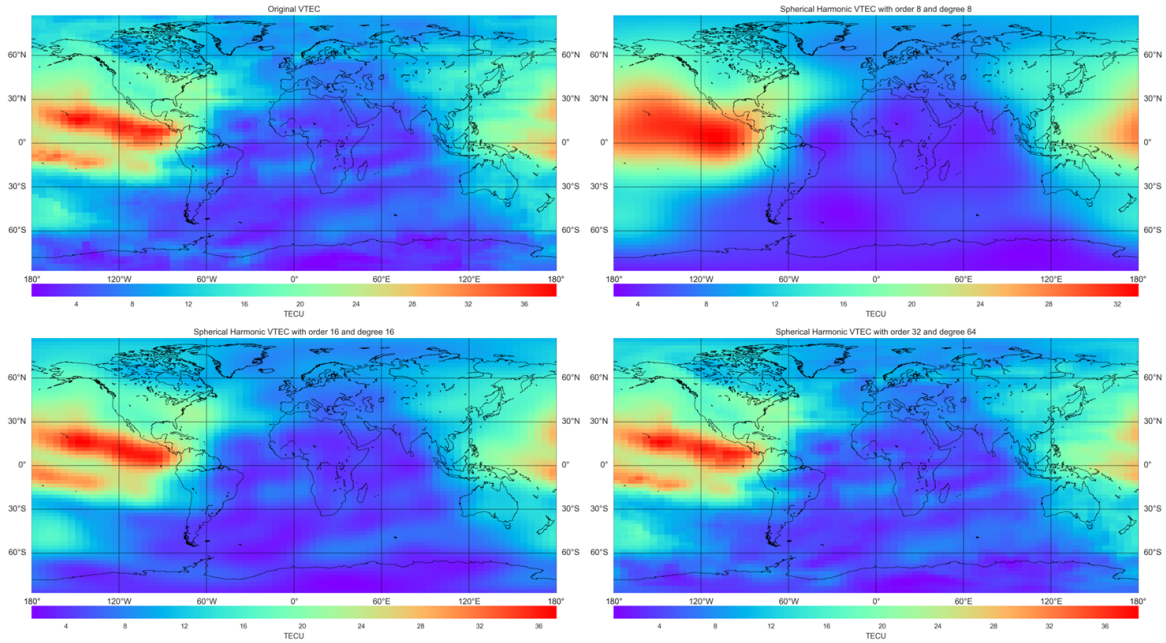

Figure 2.8 Effect of using different spherical harmonics order and degree expansion on UQRG map for day of the year 148 and year 2017. From top left to bottom right: original map, map using order and degree of 8, map using order and degree of 16 and map using degree 64 and order 32.

Chapter 3

Quality Indexes

This chapter is aimed at providing evidence of the quality of the research developed in the context of my Ph.D. study. The work supporting this thesis has been presented to a number of international conferences and peer-reviewed journals, where experts have provided valuable comments that have improved the quality and clarity of the research. The list of papers and conference proceedings can be found in the following sections.

3.1 Peer-reviewed Journals

- Hernández-Pajares, M., Roma-Dollase, D., Krankowski, A., García-Rigo, A., and Orús-Pérez, R. (2017). Methodology and consistency of slant and vertical assessments for ionospheric electron content models. *Journal of Geodesy*, 91(12):1405–1414

- Roma-Dollase, D., Hernández-Pajares, M., Krankowski, A., Kotulak, K., Ghoddousi-Fard, R., Yuan, Y., Li, Z., Zhang, H., Shi, C., Wang, C., Feltens, J., Vergados, P., Komjathy, A., Schaer, S., García-Rigo, A., and Gómez-Cama, J. M. (2018b). Consistency of seven different GNSS global ionospheric mapping techniques during one solar cycle. *Journal of Geodesy*, 92(6):691–706

- Hernández-Pajares, M., Roma-Dollase, D., Garcia-Fernàndez, M., Orus-Perez, R., and García-Rigo, A. (2018). Precise ionospheric electron content monitoring from single-frequency gps receivers. *GPS Solutions*, 22(4):102

The importance of each journal where the research has been published is proven in Table 3.1, by means of presenting the latest Impact Factor (IF) and quartile available at the time of writing this dissertation, according to Thomson Reuters. As we can see, all the previous listed journals are in the first quartile.

Journal	ISSN	Quartile	Impact Factor	5 year Impact Factor
J Geod	0949-7714	Q1	4.633	4.409
GPS Solut	1080-5370	Q1	4.727	4.767

Table 3.1 Journal information and ranking in its category based on the IF.

3.2 Conference Proceedings

- Garcia-Rigo, A., Hernandez, M., and Roma-Dollase, D. (2018a). Global distribution of ionospheric scintillations from the Real-Time GPS ROTI. In *European Geosciences Union General Assembly*, Vienna

- Hernandez-Pajares, M., Roma-Dollase, D., Garcia-Rigo, A., Krankowski, A., Fron, A., Laurichesse, D., Blot, A., and Orus-Perez, R. (2018). Assessment methodology for global ionospheric maps of electron content and potential adaptation to real-time

- Garcia-Rigo, A., Roma-Dollase, D., Hernandez, M., Li, Z., Wang, N., Terkildsen, M., Olivares, G., Ghoddousi-Fard, R., Erdogan, E., Dettmering, D., Haralambous, H., Beniguel, Y., Berdermann, J., Kriegel, M., Krypiak-Gregorczyk, A., Gulyaeva, T., Komjathy, A., Vergados, P., Feltens, J., Zandbergen, R., Fuller-Rowell, T., Altadill, D., Blanch, E., Bergeot, N., Chevalier, J. M., Krankowski, A., Agrotis, L., Galkin, I., and Orus-Perez, R. (2018b). Towards RT assessment of ionospheric monitoring within IAG's RTIM-WG. In *European Geosciences Union General Assembly*, Vienna

- Garcia-Rigo, A., Roma-Dollase, D., Hernandez, M., Li, Z., Terkildsen, M., Ghoddousi-Fard, R., Dettmering, D., Erdogan, E., Haralambous, H., Beniguel, Y., Berdermann, J., Kriegel, M., Krypiak-Gregorczyk, A., Gulyaeva, T., Komjathy, A., Vergados, P., Feltens, J., Zandbergen, R., Olivares, G., Fuller-Rowell, T., Altadill, D., Blanch, E., Bergeot, N., Krankowski, A., Agrotis, L., Galkin, I., Orus-Perez, R., and Prol, F. (2017). St. Patrick's day 2015 geomagnetic storm analysis based on real time ionosphere monitoring. In *European Geosciences Union General Assembly*, volume 19 of *EGU General Assembly Conference Abstracts*, Vienna

- Schmidt, M., Garcia-Rigo, A., Erdogan, E., Gross, A., Roma Dollase, D., and Hernandez, M. (2017). Assessment and comparisons of ionospheric vertical total electron content products. In *Joint Scientific Assembly of the International Association of Geodesy and International Association of Seismology and Physics of the Earth's Interior*, Koba

- Hernandez, M., Garcia-Rigo, A., Roma Dollase, D., Fernandez, C., Arribas, J., Majoral, M., and Vilà, J. (2017a). Some applications of ionospheric and geodetic models supported by real-time GNSS measurements. In *Reunión Sistema de Referencia Geocéntrico para Las Américas*, pages 1–37, Mendoza, Argentina

- Roma Dollase, D., Hernandez, M., and Garcia-Rigo, A. (2017). Some GNSS ionospheric monitoring techniques implemented in real-time and rapid latencies at global and polar scales. In *Mutual benefits between atmospheric research and radio based science over polar regions*, pages 1–56, Brussels

- García-Rigo, A., Roma-Dollase, D., Hernández-Pajares, M., Li, Z., Terkildsen, M., Olivares, G., Ghoddousi-Fard, R., Dettmering, D., Erdogan, E., Haralambous, H., Béniguel, Y., Berdermann, J., Kriegel, M., Krypiak-Gregorczyk, A., Gulyaeva, T., Komjathy, A., Vergados, P., Feltens, J., Zandbergen, R., Fuller-Rowell, T., Altadill, D., Bergeot, N., Krankowski, A., Agrotis, L., Galkin, I., Orus-Perez, R., and Blanch, E. (2017). Contributions to real time and near real time Ionosphere Monitoring by IAG's RTIM-WG

- Hernandez, M., Roma Dollase, D., and Garcia-Rigo, A. (2017b). Examples of IGS real-time Ionospheric information benefits: space weather monitoring, precise farming and RT-GIMs. In *International GNSS Service Workshop*, pages 1–19, Paris

- García-Rigo, A., Roma-Dollase, D., Hernández-Pajares, M., Li, Z., Terkildsen, M., and Ghoddousi-Fard, R. (2016). RTIM-WG: IAG's real time ionosphere monitoring working group: current status, outcomes and first results

- Roma Dollase, D., Hernández Pajares, M., García Rigo, A., Laurichesse, D., Schmidt, M., Erdogan, E., Yuan, Y., Li, Z., Gómez-Cama, J. M., and Krankowski, A. (2016). Real time global ionospheric maps: a low latency alternative to traditional GIMs. In *19th International Beacon Satellite Symposium (BSS 2016): Trieste, Italy: 27 june-1 july, 2016: book of abstracts*, page 1

- Hernández Pajares, M., Roma Dollase, D., Krankowski, A., García Rigo, A., and Orús Pérez, R. (2016). Comparing performances of seven different global vtec ionospheric models in the igs context. In *International GNSS Service Workshop (IGS 2016): Sydney, Australia: february 8-12, 2016*, pages 1–13. International GNSS Service (IGS)

- Roma Dollase, D., López Cama, J. M., Hernández Pajares, M., and García Rigo, A. (2015). Real-time global ionospheric modelling from gnss data with rt-tomion model.

In *5th International Colloquium Scientific and Fundamental Aspects of the Galileo Programme, 27-29 October 2015, Braunschweig, Germany*, pages 1–1. European Space Agency (ESA)

Chapter 4

Conclusions and future work

The present chapter brings together the conclusions achieved in this dissertation. In addition, future research work in progress are explained.

4.1 Conclusions

The first major accomplishment within the framework of my Ph.D. thesis was my contribution to the definition and validation of a truly independent, well established approach, using different source input data and applicable to a global scale GIM validation methodology. This methodology is based on two techniques: VTEC-altimeter data and dSTEC GPS data. The VTEC-altimeter data comparison allows assessing the GIM versus a fully independent input data with a very good coverage far away from the GNSS permanent station data (over oceans) usually used by GIMs. On the other hand, the dSTEC GPS test, has much higher accuracies and has, with slight modifications, a long history in GIMs validation. But since the input data is the same type used usually for GIMs computation, special care must be taken to not use the same station. If not done in this way, we will be assessing the residual modelling error of the GIM instead of the VTEC error on a larger scale, making all further comparison unfair with regards to other GIMs that didn't make use of this station input data. Finally, this two techniques were proven to provide correlated results of TEC. This was done comparing the dSTEC-GPS on a set of receivers on islands with altimeter data of the surrounding ocean waters.

The second major point was, in collaboration with the IAACs, to apply the previous methodology on the different GIMs provided by IGS, the combined IGS GIM and new institutes who wanted to join the IGS effort on GIM generation. The first part of this study summarizes the state-of-art GIM computation techniques currently used by the international scientific community. Afterwards, the VTEC-altimeter test is applied starting from end

of 2001 to beginning of 2016. This larger period, where TOPEX, JASON and JASON-2 altimeter data was used, allows observing the global TEC variation due to the Solar cycle and seasonal effects. Hence, the error of GIMs have been assessed in very different environmental conditions, resulting in errors as low as 2 TECUs on calm periods and as high as 10 TECUs on higher activity periods and depending on the GIM used. Finally, the dSTEC tests was done for the data of 50 permanent receivers globally distributed for the two equinox and solstice days of 2015. Afterwards, the mean results were interpolated for the entire globe, allowing an assessment of the spatial distribution of the GIMs performance. The results show that the error is higher at mid and high latitude, as expected with the higher ionospheric activity in this regions, and in the Southern Hemisphere, probably due to the large areas present there without enough permanent stations.

Another major effort was updating the already existing TOMION software to allow using multi-GNSS data and not only GPS data as until then. This was successfully accomplished for Galileo and Beidou, allowing even generating GIMs using Galileo only data. The new feature was used in demonstrating the potential extension of the capabilities of the new sidereal day filtered ionospheric GRAPHIC combination, in the detection of the Solar eclipse footprint of the 21^{th} of August 2017 over North America. In this last paper, we show that this combination may be specially useful for using single-frequency receivers for precise ionospheric sounding.

Finally, in the frame of the real-time GIM computation, two major developments have been done. First, the data acquisition software was fully rewritten to automatically classify and select the best current set of available stations. Second, a new VTEC distribution system was implemented to send the URTG map over NTRIP. This two new capabilities, plus our large experience in GIMs validation, were then successfully applied to the effort lead by UPC to create a first combined real-time map in the frame of IGS.

4.2 Future work

The post-processing TOMION software has been successfully updated to allow using multi-GNSS data, but it is still pending to include equivalent changes to the real-time processing software. The data acquisition software of the real-time software is already capable but currently deactivated until the full processing chain is ready. On the other hand, the new long name convention adopted by the IGS real-time casters, requires also defining a new methodology to identify unmistakably but being compatible with the old processing structure. Finally, the changes in the TOMION software require also an in-depth long term assessment,

specially to validate the expected performance improvement of a GIM using Galileo data, which might also deserve publication in another paper.

A new DCB computation methodology has been also implemented, specially useful for GNSS constellation with a low number of available satellites and/or permanent stations. The current method used by TOMION discards all stations that lack data of some of the satellites, reducing considerably the amount of data available for systems like Beidou, which currently still has a small number of satellites and stations. This new method needs to be further tested and later being included inside TOMION.

Finally, a first real-time combination between the real-time GIMs generated by the CNES, CAS and UPC has been implemented and validated. Still, the weighting system currently implemented may allow some improvement and different possible techniques has been identified which still need to be implemented and assessed. Specially promising may be generating directly the weight in spherical harmonics. This will allow a much more effective way to combine the maps coefficients directly, without the need of first converting the maps to IONEX and then back to spherical harmonics, which is the current real-time GIMs dissemination format.

Chapter 5

Publications

The present chapters includes a copy of the articles published in peer-reviewed journals realized in the context of my Ph.D. study.

ATTENTION¡¡

Pages 38 to 76 of the thesis, containing these articles:

- **Hernandez-Pajares, M., Roma-Dollase, D., Krankowski, A., Garcia-Rigo, A., and Orus-Perez, R**. (2017). *Methodology and consistency of slant and vertical assessments for ionospheric electron content models*. Journal of Geodesy, 91(12):1405–1414
  https://link.springer.com/article/10.1007/s00190-017-1032-z

- **Roma-Dollase, D., Hernandez-Pajares, M., Krankowski, A., Kotulak, K., Ghoddousi-Fard, R., Yuan, Y., Li, Z., Zhang, H., Shi, C., Wang, C., Feltens, J., Vergados, P., Komjathy, A., Schaer, S., Garcia-Rigo, A., and Gomez-Cama, J. M**. (2018b). *Consistency of seven different GNSS global ionospheric mapping techniques during one solar cycle*. Journal of Geodesy, 92(6):691–706
  https://link.springer.com/article/10.1007/s00190-017-1088-9

- **Hernandez-Pajares, M., Roma-Dollase, D., Garcia-Fernandez, M., Orus-Perez, R., and Garcia-Rigo, A.** (2018). *Precise ionospheric electron content monitoring from single-frequency gps receivers*. GPS Solutions, 22(4):102
  https://link.springer.com/article/10.1007/s10291-018-0767-1

are available at the mentioned editor's web

Bibliography

Dow, J., Neilan, R., and Rizos, C. (2009). The international gnss service in a changing landscape of global navigation satellite systems. Journal of Geodesy special issue, "The International GNSS Service (IGS) in a Changing Landscape of Global Navigation Satellite Systems," Vol. 83, Nos. 3-4, 2009, pp. 191–198.

Feltens, J. (2007). Development of a new three-dimensional mathematical ionosphere model at European Space Agency/European Space Operations Centre. *Space Weather*, 5(12).

Garcia-Rigo, A., Hernandez, M., and Roma-Dollase, D. (2018a). Global distribution of ionospheric scintillations from the Real-Time GPS ROTI. In *European Geosciences Union General Assembly*, Vienna.

Garcia-Rigo, A., Roma-Dollase, D., Hernandez, M., Li, Z., Terkildsen, M., Ghoddousi-Fard, R., Dettmering, D., Erdogan, E., Haralambous, H., Beniguel, Y., Berdermann, J., Kriegel, M., Krypiak-Gregorczyk, A., Gulyaeva, T., Komjathy, A., Vergados, P., Feltens, J., Zandbergen, R., Olivares, G., Fuller-Rowell, T., Altadill, D., Blanch, E., Bergeot, N., Krankowski, A., Agrotis, L., Galkin, I., Orus-Perez, R., and Prol, F. (2017). St. Patrick's day 2015 geomagnetic storm analysis based on real time ionosphere monitoring. In *European Geosciences Union General Assembly*, volume 19 of *EGU General Assembly Conference Abstracts*, Vienna.

Garcia-Rigo, A., Roma-Dollase, D., Hernandez, M., Li, Z., Wang, N., Terkildsen, M., Olivares, G., Ghoddousi-Fard, R., Erdogan, E., Dettmering, D., Haralambous, H., Beniguel, Y., Berdermann, J., Kriegel, M., Krypiak-Gregorczyk, A., Gulyaeva, T., Komjathy, A., Vergados, P., Feltens, J., Zandbergen, R., Fuller-Rowell, T., Altadill, D., Blanch, E., Bergeot, N., Chevalier, J. M., Krankowski, A., Agrotis, L., Galkin, I., and Orus-Perez, R. (2018b). Towards RT assessment of ionospheric monitoring within IAG's RTIM-WG. In *European Geosciences Union General Assembly*, Vienna.

García-Rigo, A., Roma-Dollase, D., Hernández-Pajares, M., Li, Z., Terkildsen, M., and Ghoddousi-Fard, R. (2016). RTIM-WG: IAG's real time ionosphere monitoring working group: current status, outcomes and first results.

García-Rigo, A., Roma-Dollase, D., Hernández-Pajares, M., Li, Z., Terkildsen, M., Olivares, G., Ghoddousi-Fard, R., Dettmering, D., Erdogan, E., Haralambous, H., Béniguel, Y., Berdermann, J., Kriegel, M., Krypiak-Gregorczyk, A., Gulyaeva, T., Komjathy, A., Vergados, P., Feltens, J., Zandbergen, R., Fuller-Rowell, T., Altadill, D., Bergeot, N., Krankowski, A., Agrotis, L., Galkin, I., Orus-Perez, R., and Blanch, E. (2017). Contributions to real time and near real time Ionosphere Monitoring by IAG's RTIM-WG.

Ghoddousi-Fard, R. (2014). GPS ionospheric mapping at Natural Resources Canada. In *IGS Workshop, Pasadena*.

Hernandez, M., Garcia-Rigo, A., Roma Dollase, D., Fernandez, C., Arribas, J., Majoral, M., and Vilà, J. (2017a). Some applications of ionospheric and geodetic models supported by real-time GNSS measurements. In *Reunión Sistema de Referencia Geocéntrico para Las Américas*, pages 1–37, Mendoza, Argentina.

Hernandez, M., Juan, J., and Sanz, J. (2005). *Procesado de Datos GPS: código y fase. Algoritmos, Técnicas y Recetas.* gAGE/UPC.

Hernandez, M., Roma Dollase, D., and Garcia-Rigo, A. (2017b). Examples of IGS real-time Ionospheric information benefits: space weather monitoring, precise farming and RT-GIMs. In *International GNSS Service Workshop*, pages 1–19, Paris.

Hernández-Pajares, M., Aragán-Ángel, A., Defraigne, P., Bergeot, N., Prieto-Cerdeira, R., and García-Rigo, A. (2014). Distribution and mitigation of higher-order ionospheric effects on precise gnss processing. *Journal of Geophysical Research: Solid Earth*, 119(4):3823–3837.

Hernández-Pajares, M., Juan, J., and Sanz, J. (1999). New approaches in global ionospheric determination using ground GPS data. *Journal of Atmospheric and Solar-Terrestrial Physics*, 61(16):1237–1247.

Hernández-Pajares, M., Juan, J., Sanz, J., Orus, R., García-Rigo, A., Feltens, J., Komjathy, A., Schaer, S., and Krankowski, A. (2009a). The IGS VTEC maps: a reliable source of ionospheric information since 1998. *Journal of Geodesy*, 83(3-4):263–275.

Hernández-Pajares, M., Juan, J. M., Sanz, J., Aragón-Àngel, À., García-Rigo, A., Salazar, D., and Escudero, M. (2011). The ionosphere: effects, GPS modeling and the benefits for space geodetic techniques. *Journal of Geodesy*, 85(12):887–907.

Hernández-Pajares, M., Juan, J. M., Sanz, J., Orus, R., Garcia-Rigo, A., Feltens, J., Komjathy, A., Schaer, S. C., and Krankowski, A. (2009b). The igs vtec maps: a reliable source of ionospheric information since 1998. special IGS issue of Journal of Geodesy, 83(3-4), 263-275, http://acc.igs.org/iono/igs-maps_jog09.pdf.

Hernández-Pajares, M., Roma-Dollase, D., Garcia-Fernàndez, M., Orus-Perez, R., and García-Rigo, A. (2018). Precise ionospheric electron content monitoring from single-frequency gps receivers. *GPS Solutions*, 22(4):102.

Hernandez-Pajares, M., Roma-Dollase, D., Garcia-Rigo, A., Krankowski, A., Fron, A., Laurichesse, D., Blot, A., and Orus-Perez, R. (2018). Assessment methodology for global ionospheric maps of electron content and potential adaptation to real-time.

Hernández Pajares, M., Roma Dollase, D., Krankowski, A., García Rigo, A., and Orús Pérez, R. (2016). Comparing performances of seven different global vtec ionospheric models in the igs context. In *International GNSS Service Workshop (IGS 2016): Sydney, Australia: february 8-12, 2016*, pages 1–13. International GNSS Service (IGS).

Hernández-Pajares, M., Roma-Dollase, D., Krankowski, A., García-Rigo, A., and Orús-Pérez, R. (2017). Methodology and consistency of slant and vertical assessments for ionospheric electron content models. *Journal of Geodesy*, 91(12):1405–1414.

Li, Z., Yuan, Y., Wang, N., Hernandez-Pajares, M., and Huo, X. (2015). SHPTS: towards a new method for generating precise global ionospheric TEC map based on spherical harmonic and generalized trigonometric series functions. *Journal of Geodesy*, 89(4):331–345.

Lyu, H., Hernández-Pajares, M., Nohutcu, M., García-Rigo, A., Zhang, H., and Liu, J. (2018). The barcelona ionospheric mapping function (bimf) and its application to northern mid-latitudes. *GPS Solutions*, 22(3):67.

Mannucci, A., Wilson, B., Yuan, D., Ho, C., Lindqwister, U., and Runge, T. (1998). A Global mapping technique for GPS-derived ionospheric total electron content measurements. *Radio science*, 33(3):565–582.

Markowitz, W. (1973). Si, the international system of units. *Geophysical surveys*, 1(2):217–241.

Nischan, T. (2016). *GFZRNX - RINEX GNSS Data Conversion and Manipulation Toolbox (Version 1.05)*. GFZ Data Services.

Orus, R., Cander, L. R., and Hernández-Pajares, M. (2007). Testing regional vertical total electron content maps over europe during the 17–21 january 2005 sudden space weather event. *Radio Science*, 42(3).

Orús, R., Hernández-Pajares, M., Juan, J., and Sanz, J. (2005). Improvement of global ionospheric VTEC maps by using kriging interpolation technique. *Journal of Atmospheric and Solar-Terrestrial Physics*, 67(16):1598–1609.

Roma Dollase, D., Hernandez, M., and Garcia-Rigo, A. (2017). Some GNSS ionospheric monitoring techniques implemented in real-time and rapid latencies at global and polar scales. In *Mutual benefits between atmospheric research and radio based science over polar regions*, pages 1–56, Brussels.

Roma Dollase, D., Hernández Pajares, M., García Rigo, A., Laurichesse, D., Schmidt, M., Erdogan, E., Yuan, Y., Li, Z., Gómez-Cama, J. M., and Krankowski, A. (2016). Real time global ionospheric maps: a low latency alternative to traditional GIMs. In *19th International Beacon Satellite Symposium (BSS 2016): Trieste, Italy: 27 june-1 july, 2016: book of abstracts*, page 1.

Roma-Dollase, D., Hernandez-Pajares, M., Garcia-Rigo, A., Lyu, H., Krankowski, A., Fron, A., Laurichesse, D., Blot, A., Orus-Perez, R., Yuan, Y., and et al. (2018a). Looking for optimal ways to combine global ionospheric maps in real-time.

Roma-Dollase, D., Hernández-Pajares, M., Krankowski, A., Kotulak, K., Ghoddousi-Fard, R., Yuan, Y., Li, Z., Zhang, H., Shi, C., Wang, C., Feltens, J., Vergados, P., Komjathy, A., Schaer, S., García-Rigo, A., and Gómez-Cama, J. M. (2018b). Consistency of seven different GNSS global ionospheric mapping techniques during one solar cycle. *Journal of Geodesy*, 92(6):691–706.

Roma Dollase, D., López Cama, J. M., Hernández Pajares, M., and García Rigo, A. (2015). Real-time global ionospheric modelling from gnss data with rt-tomion model. In *5th International Colloquium Scientific and Fundamental Aspects of the Galileo Programme, 27-29 October 2015, Braunschweig, Germany*, pages 1–1. European Space Agency (ESA).

Sagiya, T. (2004). A decade of GEONET: 1994–2003—The continuous GPS observation in Japan and its impact on earthquake studies—. *Earth, planets and space*, 56(8):xxix–xli.

Schaer, S. (1999). *Mapping and predicting the earths ionosphere using the Global Positioning System. 1999. 205p*. PhD thesis, Ph. D. dissertation. University of Bern, Bern, Switzerland.

Schaer, S., Gurtner, W., and Feltens, J. (1998). Ionex: The ionosphere map exchange format version 1.

Schmidt, M., Garcia-Rigo, A., Erdogan, E., Gross, A., Roma Dollase, D., and Hernandez, M. (2017). Assessment and comparisons of ionospheric vertical total electron content products. In *Joint Scientific Assembly of the International Association of Geodesy and International Association of Seismology and Physics of the Earth's Interior*, Koba.

Tange, O. (2018). *GNU Parallel 2018*. Ole Tange.

Teunissen, P. and Montenbruck, O. (2017). *Springer Handbook of Global Navigation Satellite Systems*. Springer.

Valls-Moreno, A. (2008). Wide area real time kinematic (wartk): Usage of rtcm format, and real-time implementation. Master's thesis, Universitat Politècnica de Catalunya.

Wikimedia Commons (2018). Comparison of satellite navigation orbits.

Zhang, H., Xu, P., Han, W., Ge, M., and Shi, C. (2013). Eliminating negative VTEC in global ionosphere maps using inequality-constrained least squares. *Advances in Space Research*, 51(6):988–1000.